Supporting information

From 1D to 1D-2D-1D: new insights into Li^+ diffusion behavior in optimized MnO_2 with the cooperative effect of tunnel and interface

Yinsheng Xu[a], Yuhao Xu[a], Xue Han[a], Shengping Wang[a,*], Jingxian Yu[b,*]

[a] Faculty of Materials Science and Chemistry, China University of Geosciences, Wuhan 430074, China

[b] ARC Centre of Excellence for Nanoscale BioPhotonics (CNBP), School of Chemistry and Physics, The University of Adelaide, Adelaide, SA 5005, Australia

* Corresponding Author. spwang@cug.edu.cn; jingxian.yu@adelaide.edu.au

Table of Contents

Part 1. Supplemental experimental details

Preparation of HEMD, working electrodes, and test batteries

Electrolytic manganese dioxide (EMD, purity 91%, Xiangtan, China, IBA-26 numbered by International Battery Materials Association) was heated in a muffle furnace at 350 °C for different times with a heating rate of 5 °C min^{-1} in air and then cooled to room temperature. The heat-treated electrolytic manganese dioxide (HEMD) calcined for 0, 5, 10, 20, and 40 h was labeled HEMD-0 h, HEMD-5 h, HEMD-10 h, HEMD-20 h, and HEMD-40 h, respectively.

The working electrode was prepared by mixing 80 wt% prepared HEMD, 5 wt% colloidal graphite, 5 wt% acetylene black, and 10 wt% polytetrafluoroethylene (PTFE) binder in N-methyl-2-pyrrolidone (NMP) to form a slurry, which was then applied onto 304 stainless steel wire mesh (40 mesh, 0.1 mm of thickness) by a counterroller machine and dried at 80 °C for 24 h. The cathodes before assembly were dried in a vacuum at 210 °C for 8 h.

The CR2016 test batteries were assembled in an argon atmospheric glove box with a disc-shaped pellet (0.73 mm thickness, 15.5 mm diameter, and 0.32 g mass) as the cathode, lithium metal as the anode, Celgard 2400 as the separator, and 1 mol L^{-1} $LiClO_4$ in a 1:1 (volume ratio) mixture of propylene carbonate (PC) and dimethoxyethane (DME) as the electrolyte.

Material characterization

The structure of the materials was evaluated with X-ray diffraction (XRD, Bruker/D8-FOCUS) using filtered Cu Kα radiation (λ = 1.5405 Å) with a scanning rate of 5° min^{-1} and a step size of 0.02°. X-ray photoelectron spectroscopy (XPS) analyses were performed on a K-Alpha 1063 instrument using monochromatic Al Kα as the X-ray source. The morphology and structure of HEMD were examined by field emission high-resolution transmission electron microscopy (HRTEM, JEM-2100F). A combined differential scanning calorimetry (DSC)/TGA instrument (Mettler-Toledo, TGA/DSC STAR system) was used to study the decomposition and reaction of the precursors. A combined differential scanning calorimetry (DSC)/TGA instrument (Mettler-Toledo, TGA/DSC STAR system) was used to study the calcination process of HEMD.

Determination of Pr value and Tw by XRD

Here, we make a brief description about how to determine the Pr value and Tw. The method and more detailed process can be found in the relevant literature by Y. Chabre *et al* [1]. The broadening and shift of diffraction peaks were affected by the parameters of Pr and Tw. In fact, all the diffraction peaks were affected by Tw; however, some diffraction peaks were free from being influenced by De Wolff defects. For example, the two pairs of diffraction peaks (221/240 and 002/061) are only

affected by the microtwinning defects. Therefore, we should determine the Tw firstly according to these two pairs of diffraction peaks. First, examine pattern (Cu K*a*) in the angular ranges 55° < 2θ < 59° and 64° < 2θ < 71° where the 221/240 and 002/061 peaks are to be found. For convenience, we can analyze it in four cases.

(1) Type I: for which doublets 221/240 and 002/061 are clearly separated.

(2) Type II: for which lines 221/240 have merged but that still show two (broad) 002 and 061 reflections in the range 64° < 2θ < 71°.

(3) Type III: exhibiting only two broad and symmetrical lines in the range 54 to 71°. Another characteristic feature of patterns of this type is the near disappearance of line 130, which has become very broad and has shifted to larger diffraction angle in such a way that it is now almost hidden below the line that was formerly indexed as 021.

(4) Type IV: characterized by a first broad doublet 110/130 whose angular separation Δ2θ is only about 7° instead of the usual 12° or more. The rest of the pattern consists of a limited number of weak and broad reflections.

As shown from the XRD patterns, HEMD can be classified as type IV. For samples of types IV, a relationship is applied to obtain the Tw based on the plane 002 and 061 (Equation S1).

$$Tw = 100 - 25.20\ \Delta 2\theta \tag{S1}$$

After that, Pr value can also be caculated. The main difficulty in measuring accurate values of P, from X-ray data comes from the fact that all observables are also affected by microtwinning and must be corrected accordingly before use.

(1) Pr < 0.5

First, calculate the shift δ(Tw) of line 110 produced by microtwinning:

When Tw < 55 %,

$$\delta(Tw) = -0.0054\ Tw - 8.9 \times 10^{-5}\ Tw^2 \tag{S2}$$

When Tw ≥ 55 %, δ(Tw) = -0.56°

Then, the Pr value can be calculated from the observed position 2θ of line 110 using the following expression (Equations S3, S4).

$$Pr = 0.602\ \delta(Dw) - 0.198\ \delta^2(Dw) + 0.026\ \delta^3(Dw) \tag{S3}$$

$$\delta(Dw) = 2\theta(110) - \delta(Tw) - 21.808 \tag{S4}$$

(2) 0.5 < Pr < 0.8

In contrast to highly twinned samples, line 130 is thus reasonably well observed and Pr can be estimated from the angular separation between reflections 110 and 130 using the calibration curve from the reference. Note however that the splitting (130–110) must first be corrected for the shift due to microtwinning using the empirical expression (Equation S5).

$$\delta 2\theta(110/130)_{true} = \delta 2\theta(110/130)_{obs} - 0.022\ Tw \quad (S5)$$

(3) Pr ≥ 0.8

The Pr value can be obtained using following empirical relation (Equation S6).

$$Pr = 1 - 0.053\ \beta - 0.0043\ \beta^2 \quad (S6)$$

where β is the broadening in degrees of line 110 corrected for a possible size/strain broadening.

Electrochemical measurements

Galvanostatic discharge measurements of batteries were performed at cutoff voltages of 1.5 V at 0.1 and 0.5 mA cm^{-2} by a battery testing analyzer (LAND CT2001A). EIS was performed on an electrochemical workstation (Biologic VMP3) by applying an ac signal with an amplitude of 5 mV at 10^5-10^{-2} Hz.

Determination of the Li^+ diffusion coefficient by EIS

The Nyquist plots exhibit a semicircle in the high-frequency range and a sloped line in the low-frequency range. The semicircle represents the charge-transfer process (R_{ct}) at the solid-liquid interface, and the sloped line represents the Warburg impedance (Z_W) at a low frequency, which resulted from Li^+ diffusion in solid. The Li^+ diffusion coefficient could be calculated from the low-frequency plots based on Equations S7, S8, which follow.

$$Z' = R_e + R_{ct} + \sigma_W \omega^{-1/2} \quad (S7)$$

$$D_{Li^+} = \frac{R^2T^2}{2A^2n^2F^4C^2\sigma_W^2} \quad (S8)$$

In the above equation, $\omega(2\pi f)$ is the angular frequency in the low-frequency region, R is the gas constant, T is the temperature, A is the area of the electrode, n is the number of electrons transferred per mole of the active material involved in the electrode reaction, F is the Faraday constant, and C is the molar concentration of lithium ions.

Part 2. Computational details

Bond valence sum (BVS) calculation

The bond valence sum and bond valence energy landscape were employed to determine the lithium positions and diffusion pathways. BVS calculations were performed in the 3DBVSMAPPER program, and the isosurface levels are shown at '3.0 eV', which is a parameter used to visualize ionic pathways and not a quantitative estimation [2].

Density functional theory (DFT) calculation

Density functional theory calculations were conducted using the Perdew-Burke-Ernzerhof (PBE) exchange correlation functional with semiempirical Grimme's DFT-D3 dispersion correction [3] as implemented in the Quantum Espresso (QE) software suite (version 6.4.1) [4]. Ready-to-use ultrasoft pseudopotentials (USPP) were used with electrons from O 2s, 2p, 3p, 4s, Mn 3s, 3p, 3d, and 4s, shells explicitly included in the calculations. A+U correction term of 3 eV was used for Mn, as it has been proven to yield results that are generally in good agreement with the experimental observations. Kinetic energy cutoff values of 40 Ry and 400 Ry were chosen for the wave functions and augmented charge densities, respectively. Total energies were obtained by relaxing both atomic coordinates and cell parameters using a conjugate gradient method while maintaining the symmetries of the cell (i.e., do_cellfree = 'ibrav'). The Broyden-Fletcher-Goldfarb-Shanno (BFGS) method was employed for geometry relaxations with a force convergence threshold of 10^{-3} Ry/Bohr and an energy convergence threshold of 10^{-5} Ry. The Methfessel-Paxton smearing method was used with the smearing width set to 0.05 Ry. The minimum energy paths and activation barriers of Li diffusion along different channels were calculated by the nudged elastic band method [5]. All the structures were visualized by the VESTA program [6].

Part 3. Supporting figures

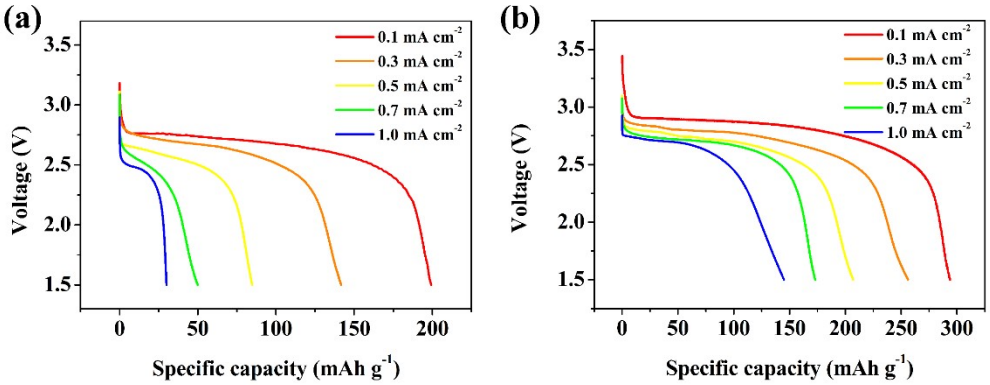

Figure S1. Discharge curves of HEMD-40 h (a) and HEMD-10 h (b) at various current densities.

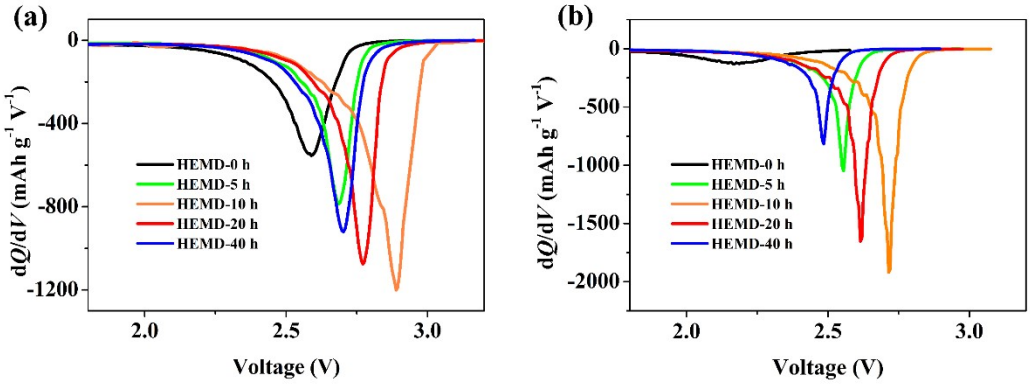

Figure S2. dQ/dV curves of HEMD at 0.1 (a) and 0.5 mA cm^{-2} (b).

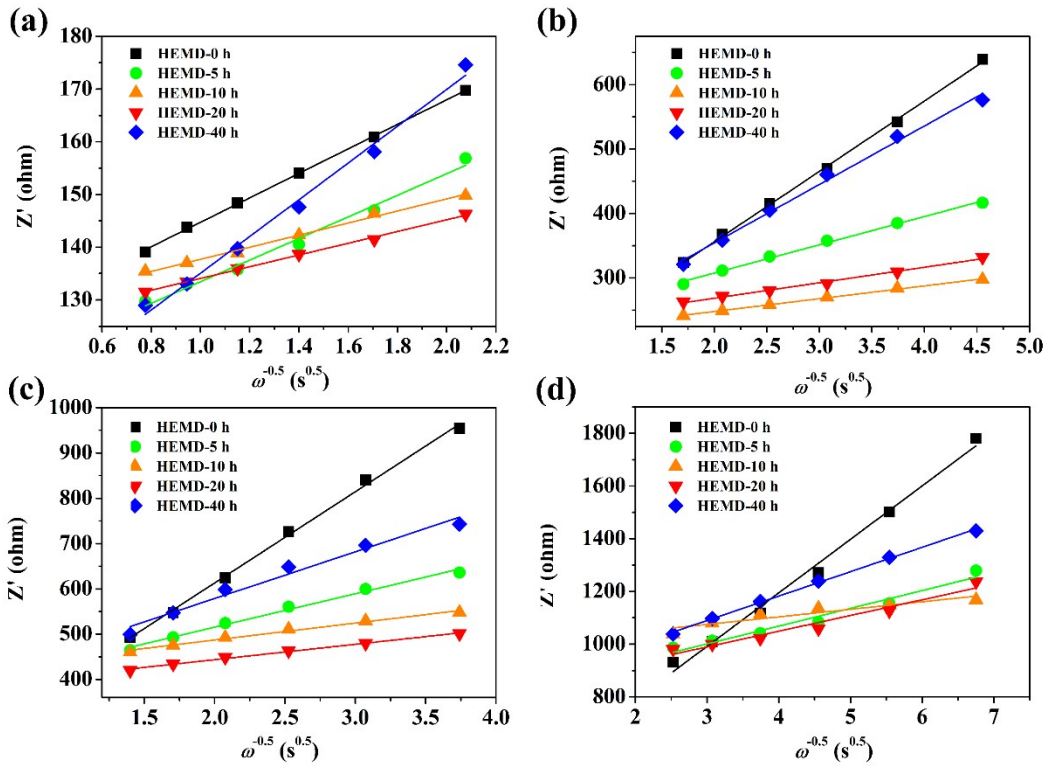

Figure S3. The relationship curves between Z' and $\omega^{-1/2}$ in the low frequency range at 0% (a), 30% (b), 60% (c), 100% (d) of depth of discharge.

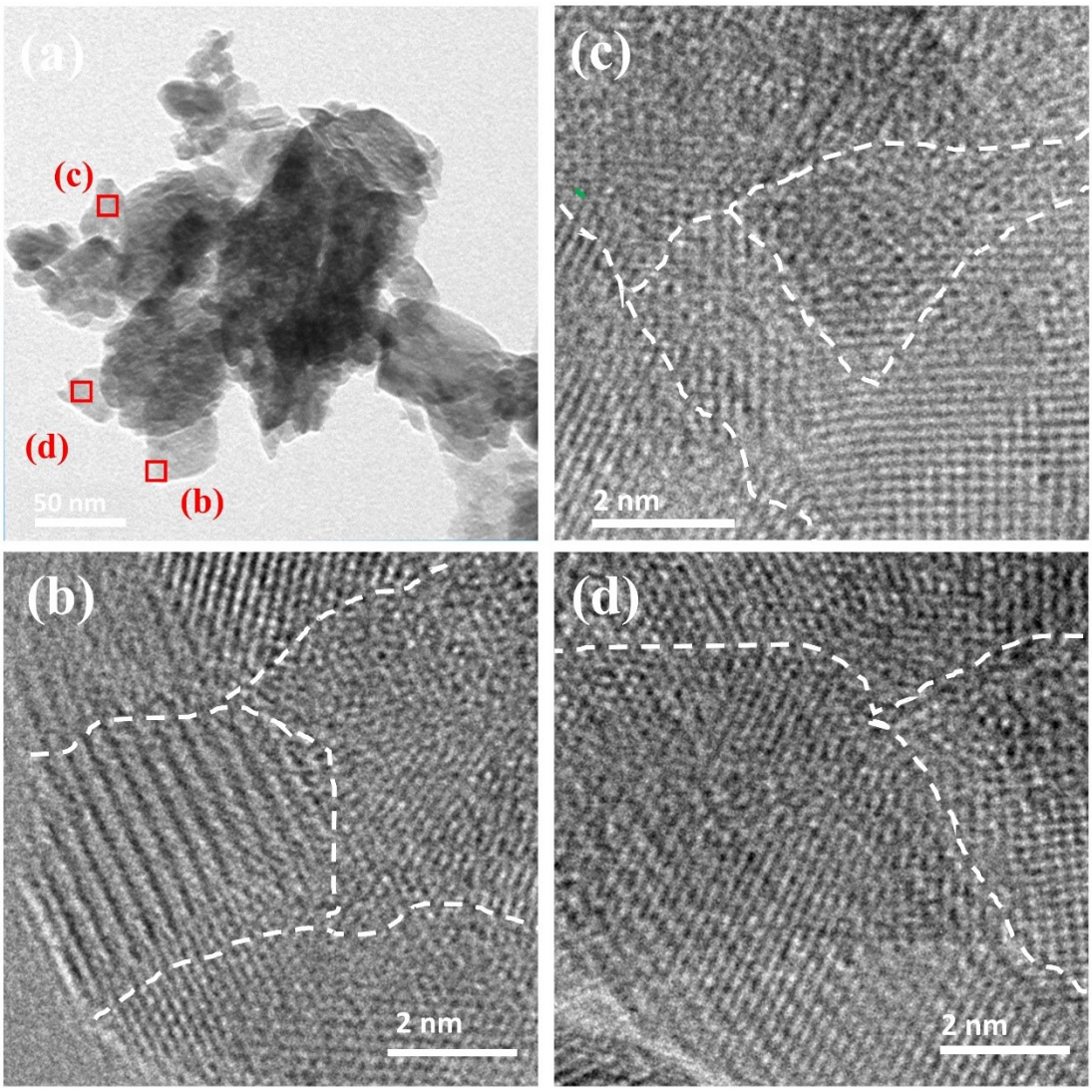

Figure S4. TEM image (a) of HEMD-0 h, and HRTEM images selected from the different regions (b-d).

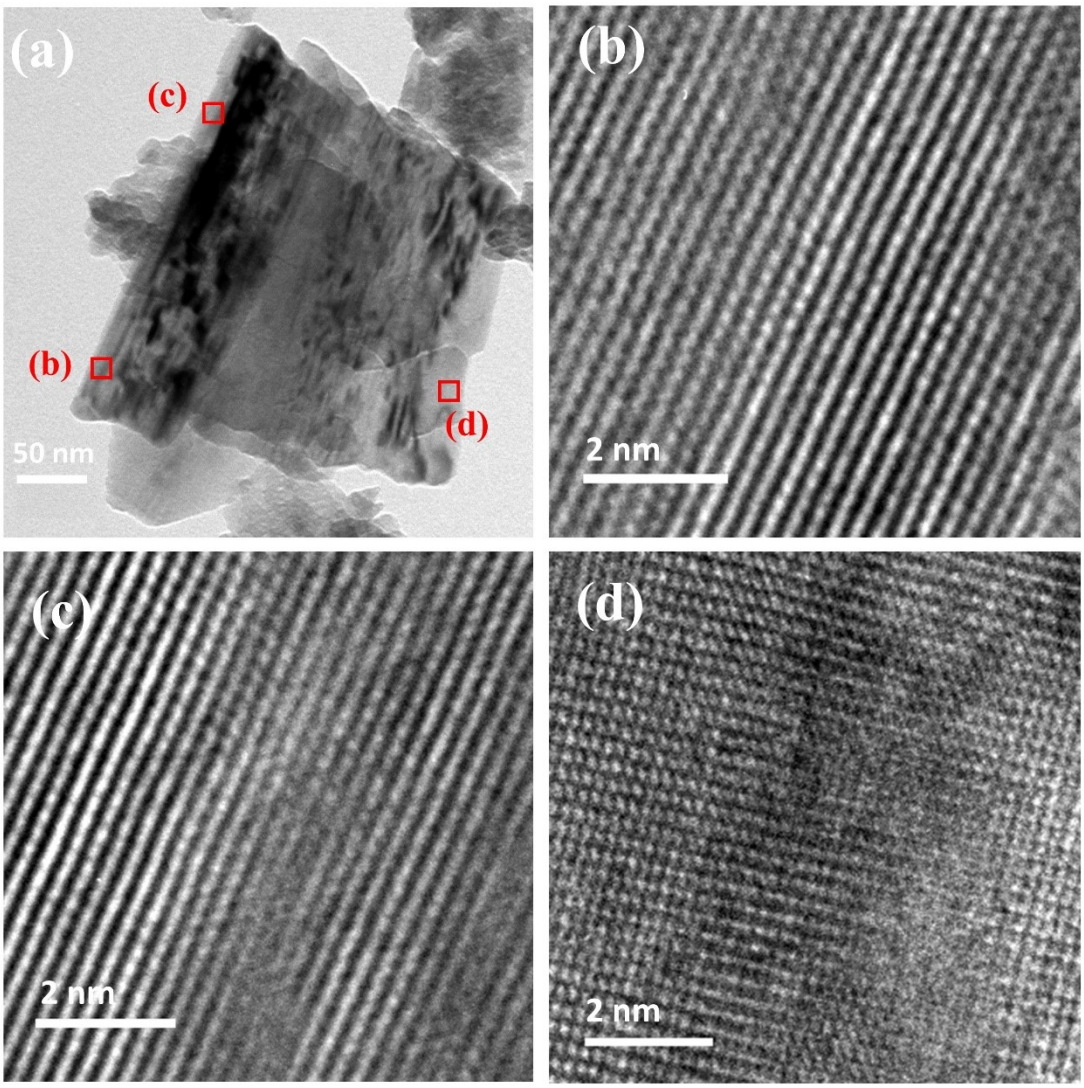

Figure S5. TEM image (a) of HEMD-40 h, and HRTEM images selected from the different regions (b-d).

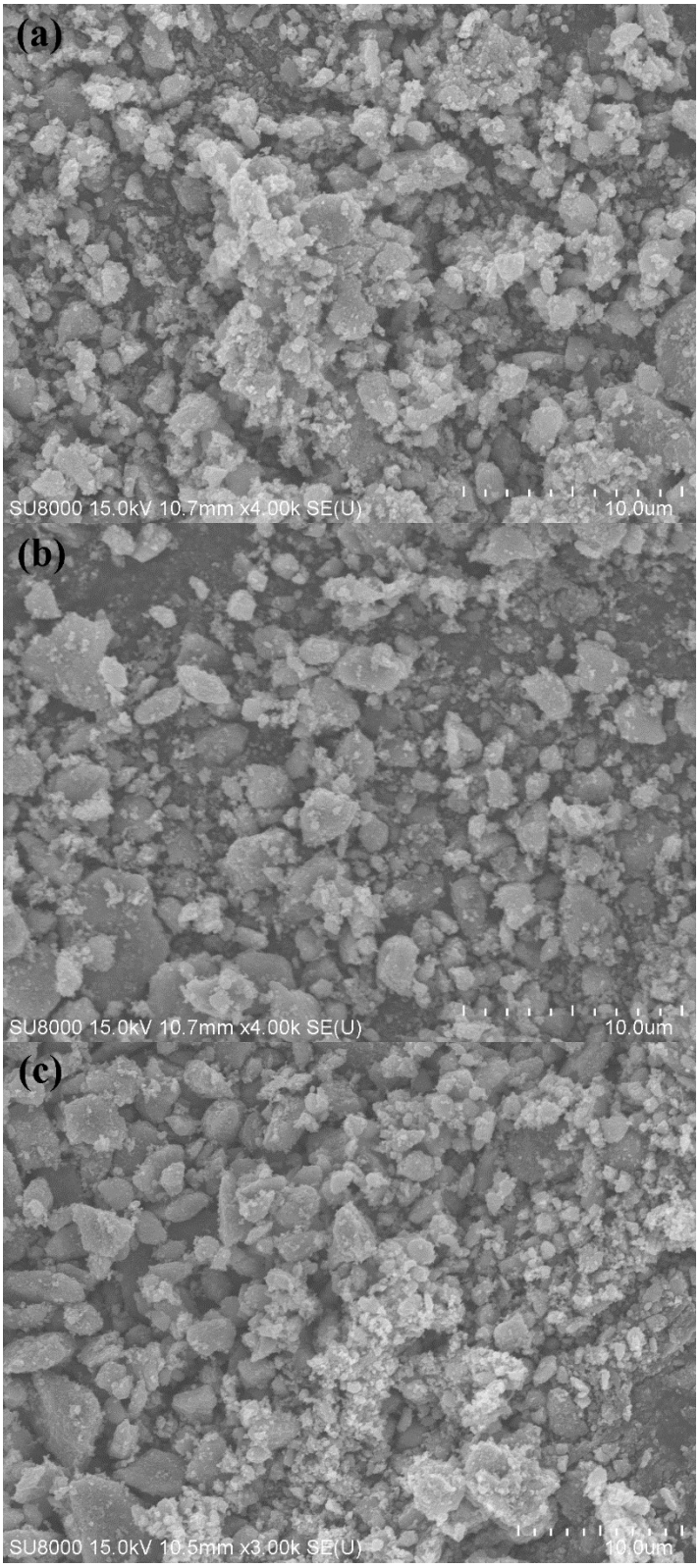

Figure S6. SEM images of HEMD-0 h (a), HEMD-10 h (b), HEMD-40 h (c).

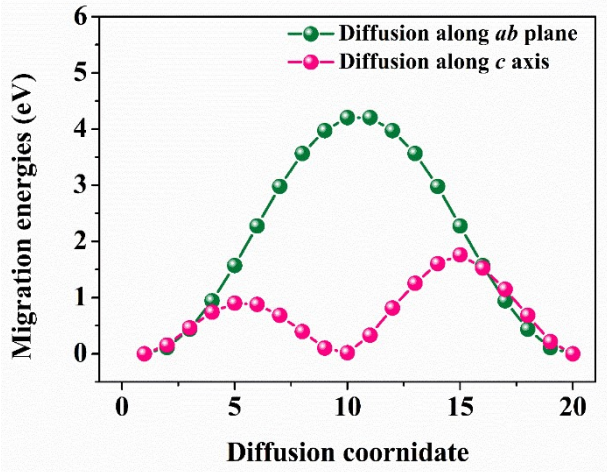

Figure S7. Migration energies of Li^+ diffusion at different directions.

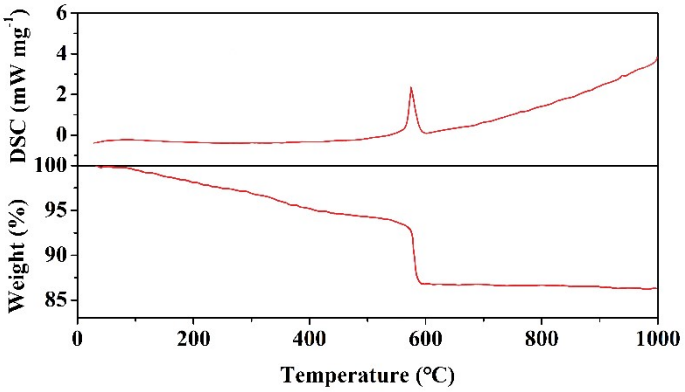

Figure S8. TG and DSC curves of EMD.

Discussion:

The transformation of composition and structure during calcination are as follows:

(1) 30-150 °C: The slow weight loss between 30 °C and 150 °C can be attributed to the loss of physically bonded water.

(2) 150-545 °C: The weight loss at these temperature range was due to the loss of structural water or chemically bonded water.

(3) 545-595 °C: The significant weight loss shown on the TG curve and a corresponding exothermal peak on the DTA curve between 545 °C and 595 °C were related to the decomposition of γ-MnO_2. According to early studies, γ-MnO_2 was decomposed into Mn_2O_3 at this temperature.

References

[1] Y. Chabre, J. Pannetier, Structural and electrochemical properties of the proton/γ-MnO_2 system, *Prog. Solid State Chem.*, **1995**, 23, 1-130. https://doi.org/10.1016/0079-6786(94)00005-2

[2] M. Sale, M. Avdeev, 3DBVSMAPPER: a program for automatically generating bond-valence sum landscapes, *Journal of Applied Crystallography*, **2012**, 45, 1054-1056. https://doi.org/10.1107/S0021889812032906

[3] L. Goerigk, S. Grimme, A thorough benchmark of density functional methods for general main group thermochemistry, kinetics, and noncovalent interactions, *Physical Chemistry Chemical Physics*, **2011**, 13, 6670-6688. https://doi.org/10.1039/c0cp02984j

[4] P. Giannozzi, S. Baroni, N. Bonini, M. Calandra, R. Car, C. Cavazzoni, D. Ceresoli, G.L. Chiarotti, M. Cococcioni, I. Dabo, A.D. Corso, S. de Gironcoli, S. Fabris, G. Fratesi, R. Gebauer, U. Gerstmann, C. Gougoussis, A. Kokalj, M. Lazzeri, L. Martin-Samos, N. Marzari, F. Mauri, R. Mazzarello, S. Paolini, A. Pasquarello, L. Paulatto, C. Sbraccia, S. Scandolo, G. Sclauzero, A.P. Seitsonen, A. Smogunov, P. Umari, R.M. Wentzcovitch, Quantum espresso: a modular and open-source software project for quantum simulations of materials, *Journal of Physics: Condensed Matter*, **2009**, 21, 395502. https://doi.org/10.1088/0953-8984/21/39/395502

[5] G. Henkelman, B.P. Uberuaga, H. Jónsson, A climbing image nudged elastic band method for finding saddle points and minimum energy paths, *The Journal of chemical physics*, **2000**, 113, 9901-9904. https://doi.org/10.1063/1.1329672

[6] K. Momma, F. Izumi, VESTA: a three-dimensional visualization system for electronic and structural analysis, *Journal of Applied Crystallography*, **2008**, 41, 653-658. https://doi.org/10.1107/S0021889808012016